Published in final edited form as:
Nat Commun. 2011 ; 2: 294. doi:10.1038/ncomms1295.

Ligand-specific deactivation time course of GluN1/GluN2D NMDA receptors

Katie M. Vance[1], **Noriko Simorowski**[2], **Stephen F. Traynelis**[1], and **Hiro Furukawa**[2,*]

[1]Department of Pharmacology, Emory University School of Medicine, Rollins Research Center, 1510 Clifton Road, Atlanta, GA, 30322-3090, USA

[2]Cold Spring Harbor Laboratory, Keck Structural Biology Laboratory, 1 Bungtown Rd., Cold Spring Harbor, NY, 11724, USAa

Abstract

N-methyl-D-aspartate (NMDA) receptors belong to the family of ionotropic glutamate receptors that mediate a majority of excitatory synaptic transmission. NMDA receptors are comprised of two glycine-binding GluN1 subunits and two glutamate-binding GluN2 subunits, of which there are four subtypes (GluN2A-D) that determine many functional properties of the receptors. One unique property of the GluN1/GluN2D NMDA receptors is an unusually prolonged deactivation time course that lasts several seconds following the removal of L-glutamate. Here, we show by a combination of x-ray crystallography and electrophysiology that the deactivation time course of the GluN1/GluN2D receptors is influenced both by the conformational variability of the ligand-binding domain as well as the chemical structure and stereochemistry of the activating ligand. Of all ligands tested, L-glutamate and L-CCG-IV induce a significantly slower deactivation time course on the GluN1/GluN2D receptors than other agonists. Furthermore, crystal structures of the isolated GluN2D ligand-binding domain monomer in complex with various ligands reveal that the binding of L-glutamate induces a unique conformation at the back side of the ligand-binding site in proximity to the region where the transmembrane domain would be located in the intact receptors. These data suggest that the activity of the GluN1/GluN2D NMDA receptor is controlled distinctively by the endogenous neurotransmitter L-glutamate.

Keywords

ionotropic glutamate receptors; NMDA receptors; GluN1/GluN2D; x-ray crystallography; electrophysiology; deactivation; pharmacology

A majority of communication between neurons is mediated by release and reception of neurotransmitters at a specialized junction called the synapse. Upon binding to neurotransmitters, ligand-gated ion channels generate postsynaptic currents that serve as neuronal signals. This neurotransmission is a critical cellular process that dictates the strength of neuronal interactions and, therefore, is a major currency for brain development and function. In the mammalian brain, L-glutamate is a primary neurotransmitter that facilitates excitatory neurotransmission. The strength and time course of L-glutamate-mediated excitatory postsynaptic currents are determined mainly by the functional properties

*Address correspondence to: Dr. Hiro Furukawa, Cold Spring Harbor Laboratory, Keck Structural Biology Laboratory, 1 Bungtown Rd., Cold Spring Harbor, NY, 11724, USA. Tel: 516-316-8872; Fax: 516-316-8873;furukawa@cshl.edu.

Coordinates

Coordinates for GluN2D ligand-binding domain structures in complex with D- and L-glutamate, L-aspartate, and NMDA were deposited in the Protein Data Bank with accession codes, 3OEL, 3OEN, 3OEK, and 3OEM, respectively.

of ionotropic glutamate receptors (iGluRs), which can be classified into three pharmacological and gene families including α-amino-3-hydroxy-5-methyl-4-propionic acid (AMPA) receptors, kainate receptors, and NMDA receptors[1,2]. NMDA receptors deactivate significantly more slowly than non-NMDA receptors, and thus comprise the slow component of the time course of excitatory postsynaptic signals[3,4].

NMDA receptors are tetrameric ion channels composed of two GluN1 subunits and two GluN2 subunits and are unique among the iGluR family members in that activation requires concurrent binding of glycine and L-glutamate to the GluN1 and GluN2 subunits, respectively[1,2]. NMDA receptor subunits possess a modular design and are composed of an amino-terminal domain (ATD), a ligand-binding domain, a transmembrane domain that forms the ion channel pore, and an intracellular carboxyl-terminal domain. The recent crystallographic study on the full-length homomeric GluA2 receptor has revealed the overall architecture and the pattern of domain organization in the context of a tetrameric subunit arrangement for AMPA receptors[5]. In contrast, structure-function studies of NMDA receptors have lagged behind AMPA receptors, primarily due to experimental complexities stemming from the heteromeric assembly of the GluN1 and GluN2 subunits. Nevertheless, structural insights into NMDA receptor function slowly have been gained through recent crystallographic studies on the ligand-binding domains[6-9] and ATD[10,11]. The most extensive studies have been conducted on the ligand-binding domains of the GluN1/GluN2A complex[7] and the GluN3A and GluN3B subunits[9], revealing the overall bi-lobed clamshell-like architecture composed of domain 1 (D1) and domain 2 (D2) with a ligand-binding pocket at the D1-D2 cleft, similar to the structure of the non-NMDA receptor ligand-binding domains[6-8]. However, there are substantial differences in how conformational changes couple to gating of the ion channels between AMPA and NMDA receptors, indicating that the physicochemical properties of the ligand-binding domains may depend on the subunit[12].

The four distinct GluN2 subunits (GluN2A-GluN2D) provide the functional and pharmacological diversity of NMDA receptors, including differences in potency and deactivation time course[1,13]. NMDA receptors that contain the GluN2D subunit have approximately a 40-fold longer deactivation time course compared to receptors containing GluN2A[14,15]. The unique properties of the GluN2D-containing NMDA receptors are considered important both for early brain development as well as function of neurons specifically expressing the GluN2D subunits in the mature brain[16-18].

Several lines of investigation have identified factors that regulate deactivation time course in NMDA receptors. For example, some studies have suggested that the rates of ligand association and dissociation at the ligand-binding domains are the primary determinants of the deactivation time course of the neuronal and GluN2A-containing NMDA receptors, as well as AMPA and kainate receptors[7,19-21]. Furthermore, recent studies have shown that the GluN2 ATD and a linker between the ATD and D1 region of the LBD (ATD-D1 linker) influence deactivation time course[22,23], indicating that the ATD exerts significant control over deactivation in NMDA receptors. Previous single channel studies have shown that the deactivation time course of macroscopic currents of NMDA receptors is dependent upon channel burst length[4]. Indeed, alignment of individual GluN1/GluN2A and GluN1/GluN2D single channel activations produces a deactivation time course with similar time constants as macroscopic currents activated by 1 mM pulses of glutamate[15,24,25]. Moreover, burst length, and therefore deactivation time course, has been shown to depend upon a series of rate constants that describe NMDA receptor gating mechanisms and differ according to which GluN2 subunit is present within the receptor. Single channel recordings of the GluN1/GluN2D receptors indicate that the receptor has longer shut time components and at least one additional shut time component than reported for the GluN1/GluN2A receptors, while the open durations are shorter. These data suggest the GluN1/GluN2D receptors remain in

the closed state longer than the GluN1/GluN2A receptors, thus lengthening activation durations, burst length, and deactivation time course[15,23,25,26].

In this study, we measure the deactivation time course of the recombinant GluN1/GluN2D NMDA receptor currents induced by a wide range of agonists. The data show that L-glutamate elicits a much slower deactivation time course compared to other excitatory amino acids such as L-aspartate. Crystallographic studies of the isolated GluN2D ligand-binding domain monomer show a unique conformation around the hinge and D2 domains of the bi-lobed clamshell when complexed with L-glutamate compared to other ligands. Moreover, structure-based mutagenesis suggests that the differences in amino acids between the GluN2A and GluN2D ligand-binding domains may distinctively influence the time course of deactivation. These data together are consistent with the idea that the unique conformation of the L-glutamate-bound ligand-binding domains may partly underlie unusually slow deactivation time course for L-glutamate in the GluN1/GluN2D receptors.

Results

GluN1/GluN2D NMDA receptors deactivate rapidly when activated by non-L-glutamate linear agonists

To assess the dependence of the prolonged deactivation time course of the GluN1/GluN2D NMDA receptors on the structure of activating ligands, we recorded whole cell responses under voltage-clamp from HEK 293 cells expressing recombinant GluN1/GluN2D and compared the response time courses of a series of glutamate and aspartate analogues. The co-agonist glycine was present in all solutions (0.05 mM), and current responses were evoked with a 1 s pulse of 1 mM agonist. Following a 1 s pulse of 1 mM L-glutamate, the GluN1/GluN2D receptors deactivated slowly with a dual exponential time course with time constants of τ_{FAST}=930 ± 100 ms and τ_{SLOW}=3200 ± 240 ms (n=30; Fig. 1*A*; Table 1), as previously described[14,15,23]. Interestingly, the stereoisomer D-glutamate caused the receptor to deactivate much more rapidly, with time constants of τ_{FAST}=27 ± 2.4 ms and τ_{SLOW}=440 ± 120 ms (n=12), considerably faster than the deactivation time constants evoked by L-glutamate (Fig. 1*A*; Table 1).

We subsequently assessed deactivation time course for other agonists. The glutamate analogue L-homocysteate, which has been detected in the brain and may act as an endogenous neurotransmitter[27-30], also caused the GluN1/GluN2D receptor to deactivate much more rapidly than L-glutamate (Table 1). L-aspartate (τ_{FAST}=130 ± 10 ms; τ_{SLOW}=280 ± 25 ms; n=8) and D-aspartate (τ_{FAST}=99 ± 8.3 ms; τ_{SLOW}=460 ± 100 ms; n=7) had similar deactivation time constants, both of which are faster than L-glutamate (Fig. 1*A*; Table 1). This suggests that any GluN2D-containing NMDA receptor at synapses at which L-aspartate participates as a primary neurotransmitter may deactivate more rapidly than synapses at which L-glutamate is released[31-35].

GluN1/GluN2D NMDA receptors deactivate slowly when activated by cyclic agonists

Several compounds with conformationally constrained rings act as partial agonists of NMDA receptors (Table 2, Supplementary Table S1), in some cases with higher potency (i.e. lower EC_{50}) than L-glutamate[36]. We therefore tested whether compounds with three-, four-, or five-member rings could evoke a slower deactivation time course than L-glutamate (Fig. 1*B*). Agonists (plus 0.05 mM glycine) were applied in 1 s pulses at 0.1 to 1 mM concentrations to HEK 293 cells expressing GluN1/GluN2D. The most potent cyclic ligand L-CCG-IV, with a three-member ring and an EC_{50} value (36 nM) that was 10-fold lower than L-glutamate, deactivated with a time course that was not significantly different from L-glutamate (τ_{FAST}=1200 ± 290 ms; τ_{SLOW}=3200 ± 600 ms; Table 2; p>0.05 ANOVA). L-

CCG-IV had a slower τ_{FAST} and τ_{SLOW} than all other linear ligands tested. *Trans*-ACBD, with a four-member ring and similar potency to L-glutamate, deactivated significantly faster than L-glutamate with time constants of τ_{FAST}=280 ± 69 ms and τ_{SLOW}=1300 ± 320 ms (n=5) (Fig. 1*B*, Table 2; ANOVA).

The relationship between GluN1/GluN2D deactivation rate and agonist potency

Previous studies have demonstrated that the deactivation time course is correlated with the ligand EC_{50} for AMPA receptors[37]. Figure 2A shows the relationship between experimentally determined EC_{50} and τ_{SLOW} for GluN1/GluN2D receptors activated by linear ligands for which τ_{SLOW} accounted for >10% of the deactivation time course. Although it would be informative to evaluate the relationship between deactivation, agonist EC_{50}, and agonist dissociation rate using models of NMDA receptor gating, a kinetic scheme that can reproduce the low open probability, rapid rise time, slow deactivation, absence of desensitization, high glutamate potency, and single channel properties of GluN1/GluN2D is not available. Establishment of a kinetic model that accurately predicts the complex properties of the GluN1/GluN2D receptors continues to be a significant challenge in the field. We therefore utilized a model of GluN1/GluN2A receptor function previously proposed by Schorge et al. (2005)[38], as well as models of GluN1/GluN2B[39] and GluN1/GluN2C[26] function to explore the relationship between tau deactivation and EC_{50} values as the dissociation rate varied (see *Methods*). Whereas these adapted models with desensitization states removed only approximately predict the properties of GluN1/GluN2D, they nevertheless give insight into the relationship between the time course for deactivation and the EC_{50} value as the glutamate dissociation rate is varied. Figure 2*A* shows that this relationship for glutamate superimposed on experimentally determined τ_{SLOW} and EC_{50} for other linear agonists that have a sufficiently large slow component (>10%) of deactivation to allow reliable determinations of τ_{SLOW}. Although gating rates almost certainly vary among ligands, these measured parameters lie reasonably close to the predicted curve for L-glutamate. By contrast, these models do not predict measured response properties of cyclic ligands, which have fewer conformational degrees of freedom than linear agonists and whose actions may be described by association and gating rates that differ substantially from L-glutamate (Fig. 2*B*). Whereas these data show how the experimentally-determined τ_{SLOW} relates to the EC_{50} for linear ligands activating GluN1/GluN2D receptors, the adapted models do not predict a fast component of deactivation comparable to that determined experimentally for GluN1/GluN2D receptors, and thus are not appropriate to describe the dual exponential time course of GluN1/GluN2D. At present, factors that control the magnitude or relative contribution of the faster time constant describing the deactivation time course of GluN1/GluN2D receptors remain unknown.

GluN1/GluN2D deactivation time course is not influenced by desensitization

Previous studies have demonstrated that even brief pulses of agonist can induce some desensitization of the GluN1/GluN2A NMDA receptors[24]. We cannot detect any desensitization of GluN1/GluN2D macroscopic current response in whole cell recordings in response to rapid and prolonged agonist application (10-90% whole cell exchange time ~4 ms). Nevertheless, we used a paired-pulse paradigm on excised patches containing GluN1/GluN2D receptors (10-90% exchange time ~0.5 ms) to evaluate whether some receptors might still have entered a desensitized state rapidly from which they recover during deactivation. The deactivation time course of the GluN1/GluN2D receptors appears uninfluenced by desensitization using a paired-pulse protocol following a 2 ms or 4 s application of 1 mM L-glutamate and 0.05 mM glycine to excised outside-out patches. No change in the peak current amplitude or deactivation time course were observed in the second agonist application given 2-10 s after the termination of the first 2 ms or 4 s pulse of agonist (n=8; Supplementary Figure S1). Whereas it is possible that the receptor desensitizes

more rapidly than can be detected (i.e. within a few microseconds), we do not observe any evidence for desensitization of GluN1/GluN2D either during agonist application or during receptor deactivation (Supplementary Figure S1).

Crystal structures of GluN2D ligand-binding domain

In order to evaluate the idea that GluN2D may adopt unique agonist-dependent conformations that influence receptor properties such as the deactivation time course, we employed x-ray crystallography and explored the structures of the isolated GluN2D ligand-binding domain monomer in complex with four different agonists: L-glutamate, D-glutamate, L-aspartate, and NMDA. All of the crystals containing the four ligands above were grown in similar conditions and were isomorphous to one another with one GluN2D ligand-binding domain molecule per asymmetric unit (Supplementary Table S2). These crystals showed x-ray diffractions to approximately 1.9 Å (Supplementary Table S2), which resulted in structures with unambiguous electron densities for proteins, ligands, and water molecules.

The overall structure of the GluN2D ligand-binding domain has a bi-lobed clamshell-like architecture composed of domains 1 and 2 (D1 and D2; Fig. 3*A*, *B*), similar to the architecture previously observed for the GluN2A isolated ligand-binding domain[7]. The GluN2A and GluN2D structures in complex with L-glutamate can be superimposed to one another with root-mean-square deviation of 0.88 Å over 240 out of 285 possible Cα positions (Fig. 3*C*). However, there are two regions in the clamshell structures when in complex with L-glutamate that are highly distinct from one another between the two subunits: the conformation of the loop at the back side of the ligand-binding site ("hinge loop") (Fig. 3*C*); and Loop 1 tethered to the protein core by two disulfide bonds in domain D1 of the clamshell structures (Fig. 3*A*, Supplementary Figure S2). Interestingly, the structures of GluN2D in complex with NMDA, L-aspartate, and D-glutamate show similarity to GluN2A at the hinge loop (Fig. 3*D*), raising the possibility that ligands that show rapid deactivation from GluN2D produce a conformation similar to GluN2A.

The different conformations of GluN2D produced by the binding of fast and slowly deactivating ligands are shown in Figure 4. A striking feature of the GluN2D ligand-binding domain structures in complex with various ligands is the considerable difference in the conformation of the "hinge loop" between the L-glutamate-bound form and all the other forms (Fig. 4*A*). The loop spans eight residues from Ile775 to Ala782, with a large difference in Cα positions ranging from approximately 1.4 Å to 9.8 Å between the L-glutamate-bound structures and the other three structures (Fig. 4). The hinge loops in the L-aspartate-, D-glutamate-, and NMDA-bound structures have highly similar conformations to one another and interact with a structural motif containing Helix E and F mainly through hydrophobic interactions involving Tyr723, Val780, and Phe781 (Fig. 4*D*). This particular orientation of the hinge loop further stabilizes the interaction with the structural motif containing Helix D and Loop D, which is located in proximity to the Gly-Thr linker, through hydrophobic interactions mediated by a cluster of non-polar residues including Ile558, Leu690, Val780, and Phe781 (Fig. 4*D*). All of the above interactions tie the hinge loop, Helix E and F, and Helix D and loop D into one unit (Fig. 4*D*). In contrast, in the L-glutamate-bound structure those interactions are absent due to a large conformational difference in the hinge loop; instead of Helix E and F, the hinge loop is tied to Helix H through a non-polar interaction between Val780 and Ala757 (Fig. 4*E*). Furthermore, in the L-glutamate-bound structure, Helix D and loop D are highly disordered, most likely because the hinge loop in the L-glutamate-bound conformation may not be suitable to form an interaction with Loop D and thus may not be able to 'lock' the conformation of Loop D.

The local conformational change described above is unlikely to reflect crystallographic artifacts for two reasons. First, all of the crystals in complex with four ligands have been grown in the same condition and are isomorphous to each other; therefore, there is no chemical factor that favors one conformation over another. Second, no crystal contact forces the hinge loop, Helix D, E, and F, and Loop D into the observed conformations. Thus, the crystal packing around the region is sufficiently "loose" to allow conformational change within the crystal lattice. Indeed, soaking the GluN2D ligand-binding domain-L-aspartate crystals against a crystallization buffer containing L-glutamate can change the hinge conformation to that observed in the GluN2D ligand-binding domain-L-glutamate co-crystal structure.

The current study is the first that structurally shows the binding pattern of NMDA to GluN2 receptors, and thus the molecular determinants defining the selectivity for the agonist NMDA can now be clearly visualized (Fig. 5). Electron density for all of the ligands, situated at the clamshell cleft between D1 and D2, is clearly visible owing to the high-resolution x-ray diffraction data obtained for all of the crystal structures (Fig. 5*A*-*D*). The amino acid ligands tested in this study bind to GluN2D through direct polar interactions involving the main chain oxygens and nitrogens of Ser536, Thr538, Arg543, Ser714, and Thr715, which also are conserved in the binding of L-glutamate to GluN2A[7]. In addition to the conserved polar interactions, the binding of NMDA involves displacement of a water molecule (W in Figure 5*A*-*D*) by the *N*-methyl group whose placement is favored by the surrounding hydrophobic residues, Tyr755 and Val759. The equivalent residues for Tyr755 in AMPA and kainate receptors are leucine and methionine, respectively, pointing away from the binding pocket (Fig. 5*E*). The corresponding residues for Val759 are methionine in AMPA receptors and threonine in kainate receptors, which are more hydrophilic (Fig. 5*E*). Furthermore, Asp756 "folds" away from the binding pocket so that its β-carboxyl group does not interfere with the placement of the *N*-methyl group of NMDA. The aspartate residue at the 756 position is conserved among the subunits of NMDA receptors. In non-NMDA receptors, the equivalent residue of Asp756 is glutamate, whose longer side chain would collide with the *N*-methyl group and disallow the placement of an NMDA molecule in the binding pocket.

Molecular correlates of GluN1/GluN2D deactivation time course

Our data demonstrate that the deactivation time course of the GluN1/GluN2D receptors differs dramatically between currents evoked by L-glutamate and other agonists, including D-glutamate, L-aspartate, and NMDA. Surprisingly, the ligand-dependence on the relative amplitudes of the two time constants (fast and slow) describing deactivation time course observed in the GluN1/GluN2D receptors is largely absent in the GluN1/GluN2A receptors (Table 3). Furthermore, the conformation of the GluN2D ligand-binding domain structure also is dependent upon the agonist, differing when in complex with L-glutamate compared to D-glutamate, L-aspartate, and NMDA. These observations imply that the ligands induce conformational changes within the GluN2D ligand-binding domain that may be contributing factors in the regulation of the deactivation time course following agonist removal. To test this hypothesis, we measured the deactivation time courses of both D- and L-glutamate-induced currents from GluN2A and GluN2D chimeric subunits within the ligand-binding domain that were engineered based on the GluN2A and GluN2D crystal structures (Figure 6). We chose to make chimeric receptors between GluN2A and GluN2D because the GluN1/GluN2A NMDA receptors deactivate more rapidly than the GluN1/GluN2D receptors when activated by L-glutamate, providing the greatest difference in deactivation time course among all GluN2 subunits. In addition, crystal structures of the L-glutamate-bound GluN2A ligand-binding domain have been previously described[7], allowing design of chimeric receptors that minimally perturb the overall subunit architecture.

We first evaluated GluN2A-(GluN2D D1D2) chimeric receptors, which are the GluN2A subunits engineered to contain the entire ligand-binding domain (i.e. both D1 and D2 regions) of GluN2D. The GluN2A-(GluN2D D1D2) receptors had a slower deactivation time course for L-glutamate (τ_{FAST}=170 ± 35 ms; τ_{SLOW}=740 ± 230 ms; n=5) compared to wild-type GluN1/GluN2A (n=21; Table 4). By contrast, the GluN2A-(GluN2D D1D2) receptors had nearly identical time course for D-glutamate (τ_{FAST}=12 ± 1.9 ms; τ_{SLOW}=200 ± 49 ms; n=5; Supplementary Table S3) as the wild-type GluN1/GluN2A receptors (τ_{FAST}=16 ± 1.3 ms; τ_{SLOW}=280 ± 130 ms; n=7, respectively; Table 3). This observation demonstrates that the full ligand-binding domain (i.e. both regions D1 and D2) can uniquely influence the deactivation time course of the GluN1/GluN2D receptors activated by L-glutamate but not D-glutamate. Of note, the GluN2D ligand-binding domain did not fully interconvert the deactivation time course of GluN2A to that of GluN2D, consistent with the recently suggested role of the ATD in the control of deactivation[22,23].

We subsequently conducted voltage-clamp recordings of chimeric receptors containing the individual D1 or D2 domains of the GluN2D ligand-binding domain to dissect the potential contributions of the D1 and D2 regions to the change in L-glutamate deactivation time course. The GluN1/GluN2A-(GluN2D-D1) receptors, which contain the D1 domain of the GluN2D subunit, had slower deactivation time course compared to the wild type GluN1/GluN2A receptors (τ_{FAST}=98 ± 4.7 ms; τ_{SLOW}=410 ± 56 ms; n=5) (Table 4). The GluN2A-(GluN2D D2) chimeric receptor containing the GluN2D D2 domain, which includes the GluN2D hinge loop region, also deactivated more slowly than wild type GluN1/GluN2A following the removal of L-glutamate (τ_{FAST}=110 ± 5.6 ms; τ_{SLOW}=660 ± 83 ms; n=7). These data suggest that both lobes of ligand-binding domain influence the deactivation time course of the GluN1/GluN2D NMDA receptors.

Because the deactivation time course is related both to agonist unbinding and channel gating, we measured the L-glutamate EC_{50} and estimated the open probability (P_{OPEN}) using the rate of onset of MK-801 block following activation by L-glutamate and glycine[40] for chimeric NMDA receptors expressed in *Xenopus* oocytes. The estimated P_{OPEN} value of only one mutant subunit (GluN2D-K779Y,V780I) changed moderately compared to wild type GluN2D (Supplementary Table S4), consistent with previous studies showing that the ATD is the primary determinant of the P_{OPEN} of both GluN2A and GluN2D[23]. Both GluN2A-(GluN2D D1) and GluN2A-(GluN2D D2) had lower EC_{50} values for L-glutamate (EC_{50} = 0.68 ± 0.20; n=4 and EC_{50} = 1.2 ± 0.20; n=4, respectively) than GluN2A (Table 4). The potency of L-glutamate in the 1GluN2A-(GluN2D D1D2) receptors (EC_{50} = 0.44 ± 0.082; n=6) was identical to the wild type GluN2D NMDA receptors (EC_{50} = 0.48 ± 0.078; n=4), in contrast to deactivation time course, which is shifted only partially towards the value for wild type GluN2A (Table 4).

The crystal structures show that the hinge within D2 is the most structurally divergent region between the GluN2A and GluN2D ligand-binding domains, and is subject to ligand-specific conformational changes depending upon whether the ligand-binding domain is in complex with L-glutamate, D-glutamate, L-aspartate, or NMDA. Using the GluN2A and GluN2D crystal structures as a guide, we identified two residues that varied between the GluN2A and GluN2D hinge regions. We first explored whether we could transfer the slower time course of GluN2A-(GluN2D D2) chimeric receptors compared to GluN2A wild type receptors by exchanging individual residues within the structurally divergent hinge. Consistent with data from chimeric receptors, GluN2A-Y754K deactivated with a slower time course for L-glutamate (τ_{FAST}=110 ± 7.5 ms; τ_{SLOW}=950 ± 150 ms; n=20; Table 5) and a slower deactivation time course for D-glutamate (τ_{FAST}=27 ± 1.4 ms; τ_{SLOW}=400 ± 130 ms; n=8; Supplementary Table S5) compared to wild-type GluN2A. Changes in deactivation time course do not appear to be dependent upon increasing or decreasing open probability,

because estimates of P_{OPEN} were unchanged for GluN2A-Y754K compared to wild type GluN2A (Supplementary Table S4). These data suggest that bringing some elements of the GluN2D hinge region into GluN2A can slow deactivation. By contrast, exchanging both divergent residues in GluN2A did not significantly alter deactivation time course (Table 5). Furthermore, the reverse experiment of moving the divergent residues in the GluN2A hinge region into GluN2D does not accelerate the deactivation, but rather either is without effect or causes a significant lengthening of deactivation compared to wild type GluN2D (Table 5, Table S4). These data show that the structurally divergent region, while capable of influencing deactivation, by itself cannot fully account for differences in deactivation rates observed in the GluN2A-(GluN2D D2) chimeric receptors. This is consistent with the idea that the structural determinants of deactivation within these multimeric receptors are complex, and may involve parts of the ligand-binding domain outside the hinge region and perhaps in parts of receptor not included in the crystal structures studied here.

Discussion

One of the remarkable characteristics of NMDA receptors is the large difference in rates of deactivation among NMDA receptors containing different GluN2 subunits, with the most prominent difference occurring between the GluN2A- and GluN2D-containing NMDA receptors. An exceptionally slow rate of deactivation is a hallmark of the GluN1/GluN2D NMDA receptors and may be important for brain development in the early stages of life. Here we show that L-glutamate, but not other linear agonists, produces both a unique conformation and exceptionally slow deactivation in the GluN1/GluN2D NMDA receptors. The relationship between EC_{50} values and deactivation rates involves gating, and thus is complex[41-44]. For the GluN1/GluN2D receptors (but not the GluN1/GluN2A receptors), the relative contribution of the fast and slow exponential components describing deactivation varies widely. Furthermore, data from the chimeric GluN1/GluN2A receptors containing the GluN2D ligand-binding domain suggest that the relationship between potency and deactivation is dependent upon ligand stereochemistry.

Variation in ligand structure has long been known to alter deactivation rates of ligand gated ion channels, first being described in classical studies of the muscle nicotinic receptor. For example, the deactivation time course of end-plate currents is accelerated by the release of the false neurotransmitter acetylmonoethylcholine, which shows brief channel open time compared to acetylcholine[45]. Similar experiments with D-glutamate in cultured hippocampal neurons also illustrate the dependence of deactivation rate on the activating ligand[46]. Furthermore, multiple studies on native and recombinant NMDA receptors have described an agonist-dependence of deactivation rate and single channel properties, including mean open time and shut time durations[4,21,47,48]. However, what appear unique about GluN2D are the marked structural changes in the isolated GluN2D ligand-binding domain when bound to L-glutamate compared to other ligands as well as the GluN2A ligand-binding domain. The recently published crystal structure of a full-length tetrameric AMPA receptor has established that the isolated ligand-binding domains accurately represent the extracellular domains in the intact receptors[5]. Therefore, although there may be a minor difference in the orientation of the hinge residues between the full-length GluN1/GluN2D receptors and the isolated GluN2D ligand-binding domain, the divergence of this region for L-glutamate compared to other agonists suggests that L-glutamate induces unique intra-protein interactions within GluN2D compared to other linear ligands bound to GluN2D or L-glutamate bound to GluN2A

Accumulating evidence indicates that multiple regions of the GluN2 subunits are involved in regulation of the deactivation time course. Recent studies have shown that the amino terminal domain (ATD) and the sixteen amino acid linker between the ATD and ligand-

binding domain (ATD-D1 linker) are critical regions that control deactivation rate as well as open probability. Substitutions of the ATD or ATD-D1 linker from GluN2A with that from GluN2D result in approximately a 6-fold or 2-fold increase in deactivation time course, respectively[22,23]. In the current study, we show that the substitution of the ligand-binding core of GluN2A with that of GluN2D also slows the deactivation time course for L-glutamate to a similar degree as the ATD substitution (Table 3). Evaluation of individual domains D1 and D2 as well as individual residues in the structurally divergent hinge region suggest that the structural determinants of deactivation within the ligand binding domain are broadly distributed. Thus, in addition to the ATD, we propose that the ligand-binding domain is also an important determinant of the deactivation process for L-glutamate[36,49]. Remarkably, the GluN2D ligand-binding domain does not control the deactivation time course of D-glutamate-induced currents, indicating that the ligand-binding domain of GluN2D may distinctively sense L-glutamate from other linear ligands.

Previous studies on the glutamate receptor ligand-binding cores have indicated that opening and closing of the bilobed clamshell structure upon ligand-binding and -unbinding translate into the major physical driving force for gating of ion channel pores[50-52]. The crystallographic analyses conducted here show that the extent of domain closure between D1 and D2 in the GluN2D ligand-binding domain structures is nearly identical to each other when complexed with the four linear ligands including L- and D-glutamate, L-aspartate, and NMDA. However, a substantial difference in conformation is observed in the region containing the hinge loop at the back side of the ligand-binding site, including Helix D, E, F, and Loop D in domain D2 between the structures in complex with L-glutamate and other ligands. The conformation of the hinge loop in the L-glutamate-bound form is such that the residues can no longer interact with Helix D and Loop D, making them highly disordered or flexible. It is plausible that this change in Helix D and Loop D orientation can affect gating properties (and thus deactivation time course) because they are in proximity to the region where transmembrane helices are tethered in the intact receptors.

The hinge region may also be important for “sensing” L-glutamate, even though it is not directly involved in binding, because deactivation rates of D-glutamate-induced currents are not changed in the chimeric or mutant receptors for which this region is altered. In the GluN1 subunit, a similar site has been shown to be important for discriminating partial agonists from full-agonists[12]. The equivalent structural motifs involving the hinge loop (Strand 14 in GluN1) and Helix E and F (Helix F and G in GluN1) in GluN1 ligand-binding domain have conformational variability between the glycine-bound and partial agonist-bound forms, thereby serving as a “sensor” for discriminating types of ligands and regulating the open probability of the ion channel.

Methods

Molecular Biology

cDNAs for the recombinant rat wild type NMDA receptor subunits GluN1-1a (GenBank U11418, U08261; hereafter GluN1), GluN2A (GenBank D13211), and GluN2D (GenBank L31611) were used for electrophysiological recordings. Constructs encoding chimeric rat GluN2A and GluN2D proteins for GluN2A-(GluN2D D1D2), GluN2A-(GluN2D D1), and GluN2A-(GluN2D D2) and point mutants were developed as previously described[23,49]. All chimeric and point mutant receptors were verified by DNA sequencing. All plasmids used were subcloned into the pCI-neo vector except GluN2A (wild type), which was subcloned into the pcDNA1/AMP vector. Amino acid composition of chimeric receptors is given in Supplementary Table S6.

Two-electrode voltage-clamp recordings

Preparation and injection of cRNAs encoding the GluN1 and GluN2A, GluN2D, or GluN2A-GluN2D chimeric or mutant receptors into *Xenopus laevis* oocytes as well as all two-electrode voltage-clamp recordings were performed as previously described[53]. Briefly, oocytes were stored at 15°C in Barth's culture bath containing (in mM) 88 NaCl, 5 Tris-HCl, 2.4 $NaHCO_3$, 1 KCl, 0.82 $MgSO_4$, 0.41 $CaCl_2$, and 0.33 $Ca(NO_3)_2$ at pH 7.4. Oocytes were injected with 5-10 ng cRNAs synthesized *in vitro* from linearized template cDNA at a ratio of 1 GluN1 subunit to 2 GluN2 subunits. Recordings were performed 2-4 days post-injection at 23°C (room temperature). The external bath solution contained (in mM) 90 NaCl, 10 HEPES, 1 KCl, 0.5 $BaCl_2$, and 0.01 EDTA at pH 7.4. Voltage electrodes were filled with 0.3 M KCl, and current electrodes contained 3 M KCl. Current responses were recorded at a holding potential of -30 to -60 mV. Voltage control and data acquisition were controlled with a two-electrode voltage-clamp amplifier (OC725, Warner Instruments), and an 8-modular valve positioner (Digital MVP Valve) controlled solution exchange. Recording solutions were prepared in external bath solution and contained glycine (30 μM) and glutamate (0.1-100 μM). MK-801 (200 nM; Sigma-Aldrich) was prepared in bath solution containing glutamate (100 μM) and glycine (30 μM).

Cell Culture

Human embryonic kidney-293 cell line (CRL 1573; ATCC, Rockville, MD, USA; hereafter HEK 293) were plated on 5 mm diameter glass coverslips (Warner Instruments, Hamden, CT) coated in 100 μg/mL poly-D-lysine and were maintained in 5% humidified CO_2 at 37°C in DMEM (Dulbecco's Modified Eagle Medium Cat. No. 11960; Invitrogen, Carlsbad, CA, USA) supplemented with 10% fetal bovine serum, 10 units/ml penicillin, and 10 μg/ml streptomycin. HEK 293 cells were transiently transfected using the Fugene transfection reagent (Roche Diagnostics, Basel, Switzerland) with cDNA encoding green fluorescent protein (GFP), GluN1, and GluN2A, GluN2D, or a chimeric GluN2A-GluN2D subunit at a ratio of 1:1:1 for 0.5 μg/well total cDNA, as previously described[23]. Following transfection, cells were incubated in media supplemented with NMDA receptor antagonists D,L-2-amino-5-phosphonovalerate (200 μM) and 7-chlorokynurenic acid (200 μM).

Whole cell voltage-clamp recordings

Voltage-clamp current recordings (V_{HOLD} = -60 mV) were conducted on HEK 293 cells using an Axopatch 200B amplifier (Molecular Devices, Union City, CA, USA) and digitized by Axon pClamp10 software. Recordings were filtered at 8 kHz using an eight-pole Bessel filter (-3 dB; Frequency Devices, Haverhill, MD, USA) and digitized at 40 kHz. Thin-walled borosilicate glass (Warner Instruments, 1.5 mm/1.12 mm OD/ID, Cat. No. TW-150F-4, Hamden, CT, USA) was used to form recording micropipettes, which were filled with an internal solution containing (in mM) 110 D-gluconate, 110 CsOH, 30 CsCl, 5 HEPES, 4 NaCl, 0.5 $CaCl_2$, 2 $MgCl_2$, 5 BAPTA, 2 NaATP, and 0.3 NaGTP (pH 7.35). Cells were bathed at 23°C in external solution that contained (in mM) 150 NaCl, 10 HEPES, 30 D-mannitol, 3 KCl, 0.5 $CaCl_2$, and 0.01 EDTA at pH 8.0. Macroscopic currents were evoked from cells lifted into the path of a two-barrel theta tube by application of 0.05 mM glycine, followed by 1 s pulses of agonist solutions containing 0.05 mM glycine plus 0.1 to 1 mM L-glutamate or other GluN2 ligands, and returned to the initial 0.05 mM glycine application for 3 to 25 s. In paired-pulse experiments, GluN1/GluN2D receptors were activated by 2 ms or 4 s pulses of 1 mM L-glutamate and 0.05 mM glycine followed by a second pulse applied 2 to 10 s after the removal of the first pulse for 2 ms or 4 s. Rapid solution exchange for macroscopic recordings was accomplished with a theta pipette controlled by a piezoelectric translator (Burleigh Instruments, Fishers, NY). Whole cell 10 to 90% solution exchange times were approximately 4 ms and were determined as previously described[54], and 10 to

90% open tip solution exchange times were under 0.5 ms. Between 5 and 10 sweeps were recorded for each condition.

Data Analysis

For each macroscopic current condition, the current response waveforms recorded under voltage-clamp were aligned on the point of steepest rise and averaged following subtraction of the pre-application baseline. Current amplitude, 10% to 90% rise time, and deactivation time constant were determined. Relative maximum response was determined by expressing the response of a maximally effective concentration of a given agonist as a percentage of the response to 1 mM L-glutamate recorded in the same cell. The deactivation time constant was fit using the following equation:

Response = Amp_{FAST} (exp-time / τ_{FAST}) ± Amp_{SLOW} (exp-time / τ_{SLOW}) where τ_{FAST} is the fast deactivation time constant, τ_{SLOW} is the slow deactivation time constant, Amp_{FAST} is the amplitude of the fast deactivation component, Amp_{SLOW} is the amplitude of the slow deactivation component, and t=0 is defined as the peak of the response at the moment deactivation is initiated. Weighted deactivation time constants were determined using the following equation:

$$\tau_w = \left\{\left[Amp_{\mathrm{FAST}} / \left(Amp_{\mathrm{FAST}} + Amp_{\mathrm{SLOW}}\right)\right] \times \tau_{\mathrm{FAST}}\right\} + \left\{\left[Amp_{\mathrm{SLOW}} / \left(Amp_{\mathrm{FAST}} + Amp_{\mathrm{SLOW}}\right)\right] \times \tau_{\mathrm{SLOW}}\right\}$$

where τ_W is the weighted deactivation time constant.

Relative P_{OPEN} was estimated for chimeric receptors and point mutants by analyzing the time course for the onset of MK-801 inhibition, as previously described[40]. Briefly, the rate of onset of MK-801 inhibition was calculated using the following equation:

$$\text{Block rate}_{\mathrm{MK-801}} = 1/\tau_{\mathrm{MK-801}}$$

where $\tau_{\text{MK-801 block}}$ is the time constant of the onset of MK-801 block. $\tau_{\text{MK-801 block}}$ was calculated using the single-exponential equation

$$\text{Response} = Amp\,(\exp - \text{time}/\tau_{\mathrm{MK-801}}) + \text{sready} - \text{state}$$

where *Amp* is the amplitude of the current response and *steady-state* describes the steady-state current observed in the presence of incomplete MK801 block. Open probability (P_{OPEN}) for the chimeric receptors and point mutants were calculated from wild type receptor open probability and the block rate of MK-801 using the following equation

$$P_{\mathrm{OPEN(MUT)}} = P_{\mathrm{OPEN}}\left(\tau_{\mathrm{MK-801WT}}/\tau_{\mathrm{MK-801(MUT)}}\right)$$

where GluN2A P_{OPEN} was 0.48 and GluN2D P_{OPEN} was 0.012, determined from single channel data[23]. Concentration-response curves were fitted for each oocyte with the following Hill equation

$$\text{Percent response} = 100/\left(1 + (EC_{50}/[A])^{n_H}\right)$$

where EC_{50} is the agonist concentration that produces a half-maximal effect, and n_H is the Hill coefficient.

The responses of gating models were evaluated by numerical integration (Channelab, Synaptosoft) and assessment of the Q matrix[15] to determine the deactivation time course and EC_{50} values as a function of the agonist dissociation rates (SCALCS, HJCFIT, kindly provided by Dr. David Colquhoun, University College London). Three models were adapted as shown below to simulate NMDA receptor responses, including the GluN1/GluN2A model from Schorge et al. (2005)[38] (Scheme 1), as well as the GluN1/GluN2B model (Scheme 2) from Amico-Ruvio and Popescu (2010)[39] and the GluN1/GluN2C model (Scheme 3) from Dravid et al. (2008)[26].

Data are reported as mean ± s.e.m. and were evaluated statistically using one-way ANOVA and Tukey's *post hoc* test. Significance for all tests was set at $p < 0.05$. EC_{50} values are reported as mean ± s.e.m., but statistical analyses were performed on the $\log(EC_{50})$, as EC_{50} demonstrates a lognormal distribution[55].

Protein Purification and Crystallization

The GluN2D ligand-binding domain construct used in this structural study was defined as Asp424-Arg564 and Thr686-Asn827 connected by a Gly-Thr linker. The GluN2D ligand-binding domain protein was expressed as a fusion protein to small ubiquitin-like modifier (SUMO) with the N-terminal hexa-histidine tag in Origami B (DE3) strain (Novagen) under T7 promoter in pET22b(+) (Novagen). After growing cells to $OD_{600} = 4$ in a fermenter (BioFlo3000; New Brunswick) at 37°C, protein expression was induced by 0.5 mM IPTG at 15°C for 36 h. The GluN2D ligand-binding domain proteins were purified using Nickel-chelating Sepharose (GE Healthcare) and digested by ubiquitin ligase protease-1 to remove SUMO. The sample was further purified by a combination of Q-Sepharose, SP-Sepharose, and Superdex200 (GE Healthcare).

Structural Studies

The purified GluN2D ligand-binding domain proteins were concentrated to approximately 5 mg/ml and dialyzed against a buffer containing 10 mM Tris-HCl (pH 8), 50 mM NaCl, and 10 mM of D- and L-glutamate, L-aspartate, or NMDA. All of the crystals were produced by vapor diffusion at 17°C in hanging drops containing 2:1 protein to reservoir solution composed of 3.5-4.5 M sodium formate, 100 mM CAPS (pH 9-10), and 8-12% 1,4-butanediol. The concentration of 1,4-butanediol was raised to 14% for cryoprotection of the crystals during data collection. The x-ray diffraction data was collected at X25, X26C, and X29 beamlines at National Synchrotron Light Source at Brookhaven National Laboratory and processed using HKL2000. The structure of the L-glutamate-bound form was determined by molecular replacement using an alanine chain of the GluN2A ligand-binding domain structure (PDB code: 2A5S) as a molecular search probe and by using the program Phaser[56]. The GluN2D S1S2 structures in complex with L-aspartate, D-glutamate, and NMDA were determined by molecular replacement using the structure of GluN2D ligand-binding domain in complex with L-glutamate. Structural refinement and model building were performed with PHENIX[57] and Coot[58], respectively.

Supplementary Material

Refer to Web version on PubMed Central for supplementary material.

Acknowledgments

We thank Erkan Karakas for helps in collection of x-ray diffraction data, and Kasper Hansen and Hongjie Yuan for critical comments on the manuscript. We also thank Alasdair Gibb for advice on kinetic modeling and critical comments on the manuscript. We also thank the staffs at beamlines X25, X26C, and X29 of the National Synchrotron Light Source. This work was supported by the NINDS (NS036654, NS065371 to SFT), NIH training grants (T32-ES012870 and T32-DA01504006, KMV), NIMH (MH085926-01A1 to HF). HF is also supported by a new investigator research grant from Alzheimer's Association.

References

1. Erreger K, Chen P, Wyllie D, Traynelis S. Glutamate receptor gating. Crit Rev Neurobiol. 2004; 16:187–224. [PubMed: 15701057]
2. Traynelis SF, et al. Glutamate receptor ion channels: structure, regulation, and function. Pharmacol Rev. 2010; 62:405–496. [PubMed: 20716669]
3. Forsythe ID, Westbrook GL. Slow excitatory postsynaptic currents mediated by N-methyl-D-aspartate receptors on cultured mouse central neurones. The Journal of Physiology. 1988; 396:515–533. [PubMed: 2900892]
4. Lester RAJ, Clements JD, Westbrook GL, Jahr CE. Channel kinetics determine the time course of NMDA receptor-mediated synaptic currents. Nature. 1990; 346:565–567. [PubMed: 1974037]
5. Sobolevsky AI, Rosconi MP, Gouaux E. X-ray structure, symmetry and mechanism of an AMPA-subtype glutamate receptor. Nature. 2009; 462:745–756. [PubMed: 19946266]
6. Furukawa H, Gouaux E. Mechanisms of activation, inhibition and specificity: crystal structures of the NMDA receptor NR1 ligand-binding core. EMBO J. 2003; 22:2873–2885. [PubMed: 12805203]
7. Furukawa H, Singh SK, Mancusso R, Gouaux E. Subunit arrangement and function in NMDA receptors. Nature. 2005; 438:185–192. [PubMed: 16281028]
8. Mayer ML. Glutamate receptors at atomic resolution. Nature. 2006; 440:456–462. [PubMed: 16554805]
9. Yao Y, Harrison CB, Freddolino PL, Schulten K, Mayer ML. Molecular mechanism of ligand recognition by NR3 subtype glutamate receptors. EMBO J. 2008; 27:2158–2170. [PubMed: 18636091]
10. Hansen KB, Furukawa H, Traynelis SF. Control of assembly and function of glutamate receptors by the amino-terminal domain. Mol Pharmacol. 2010; 78:535–549. [PubMed: 20660085]
11. Karakas E, Simorowski N, Furukawa H. Structure of the zinc-bound amino-terminal domain of the NMDA receptor NR2B subunit. EMBO J. 2009; 28:3910–3920. [PubMed: 19910922]
12. Inanobe A, Furukawa H, Gouaux E. Mechanism of Partial Agonist Action at the NR1 Subunit of NMDA Receptors. Neuron. 2005; 47:71–84. [PubMed: 15996549]
13. Cull-Candy SG, Leszkiewicz DN. Role of Distinct NMDA Receptor Subtypes at Central Synapses. Sci. STKE. 2004; 2004:1–9.
14. Vicini S, et al. Functional and Pharmacological Differences Between Recombinant N-Methyl-D-Aspartate Receptors. J Neurophysiol. 1998; 79:555–566. [PubMed: 9463421]
15. Wyllie DJA, Behe P, Colquhoun D. Single-channel activations and concentration jumps: comparison of recombinant NR1a/NR2A and NR1a/NR2D NMDA receptors. J Physiol. 1998; 510:1–18. [PubMed: 9625862]
16. Standaert DG, Testa CM, Young A, Penney JB Jr. Organization of N-methyl-D-aspartate glutamate receptor gene expression in the basal ganglia of the rat. J Comp Neurol. 1994; 343:1–16. [PubMed: 8027428]
17. Monyer H, Burnashev N, Laurie DJ, Sakmann B, Seeburg PH. Developmental and regional expression in the rat brain and functional properties of four NMDA receptors. Neuron. 1994; 12:529–540. [PubMed: 7512349]
18. Momiyama A, Feldmeyer D, Cull-Candy SG. Identification of a native low-conductance NMDA channel with reduced sensitivity to Mg2+ in rat central neurones. J Physiol. 1996; 494:479–492. [PubMed: 8842006]

19. Weston MC, Gertler C, Mayer ML, Rosenmund C. Interdomain Interactions in AMPA and Kainate Receptors Regulate Affinity for Glutamate. J. Neurosci. 2006; 26:7650–7658. [PubMed: 16855092]
20. Jin R, et al. Mechanism of Positive Allosteric Modulators Acting on AMPA Receptors. J. Neurosci. 2005; 25:9027–9036. [PubMed: 16192394]
21. Lester RA, Jahr CE. NMDA channel behavior depends on agonist affinity. J. Neurosci. 1992; 12:635–643. [PubMed: 1346806]
22. Gielen M, Retchless BS, Mony L, Johnson JW, Paoletti P. Mechanism of differential control of NMDA receptor activity by NR2 subunits. Nature. 2009; 459:703–707. [PubMed: 19404260]
23. Yuan H, Hansen KB, Vance KM, Ogden KK, Traynelis SF. Control of NMDA Receptor Function by the NR2 Subunit Amino-Terminal Domain. J. Neurosci. 2009; 29:12045–12058. [PubMed: 19793963]
24. Zhang W, Howe JR, Popescu GK. Distinct gating modes determine the biphasic relaxation of NMDA receptor currents. Nat Neurosci. 2008; 11:1373–1375. [PubMed: 18953348]
25. Erreger K, Dravid SM, Banke TG, Wyllie DJA, Traynelis SF. Subunit-specific gating controls rat NR1/NR2A and NR1/NR2B NMDA channel kinetics and synaptic signalling profiles. J Physiol. 2005; 563:345–358. [PubMed: 15649985]
26. Dravid SM, Prakash A, Traynelis SF. Activation of recombinant NR1/NR2C NMDA receptors. J Physiol. 2008; 586:4425–4439. [PubMed: 18635641]
27. Do K, Herrling PL, Streit P, Cuenod M. Release of neuroactive substances: homocysteic acid as an endogenous agonist of the NMDA receptor. J Neural Transm. 1988; 72:185–190. [PubMed: 2901456]
28. Do KQ, Herrling PL, Streit P, Turski WA, Cuenod M. In vitro release and electrophysiological effects in situ of homocysteic acid, an endogenous N-methyl-(D)-aspartic acid agonist, in the mammalian striatum. J. Neurosci. 1986; 6:2226–2234. [PubMed: 2875135]
29. Olney JW, et al. L-Homocysteic acid: An endogenous excitotoxic ligand of the NMDA receptor. Brain Research Bulletin. 1987; 19:597–602. [PubMed: 2891418]
30. Yuzaki M, Connor JA. Characterization of L-Homocysteate-Induced Currents in Purkinje Cells From Wild-Type and NMDA Receptor Knockout Mice. J Neurophysiol. 1999; 82:2820–2826. [PubMed: 10561449]
31. Benveniste H. Brain Microdialysis. J Neurochem. 1989; 52:1667–1679. [PubMed: 2656913]
32. Fleck MW, Henze DA, Barrionuevo G, Palmer AM. Aspartate and glutamate mediate excitatory synaptic transmission in area CA1 of the hippocampus. J. Neurosci. 1993; 13:3944–3955. [PubMed: 7690067]
33. Nicholls D. Release of glutamate, aspartate, and gamma-aminobutyric acid from isolated nerve terminals. J Neurochem. 1989; 52:331–341. [PubMed: 2562986]
34. Wang L, Nadler JV. Reduced aspartate release from rat hippocampal synaptosomes loaded with Clostridial toxin light chain by electroporation: Evidence for an exocytotic mechanism. Neuroscience Letters. 2007; 412:239–242. [PubMed: 17123709]
35. Zhang XY, Nadler JV. Postsynaptic response to stimulation of the Schaffer collaterals with properties similar to those of synaptosomal aspartate release. Brain Research. 2009; 1295:13–20. [PubMed: 19664606]
36. Erreger K, et al. Subunit-specific agonist activity at NR2A-, NR2B-, NR2C-, and NR2D-containing N-methyl-D-aspartate glutamate receptors. Mol Pharmacol. 2007; 72:907–920. [PubMed: 17622578]
37. Zhang W, Robert A, Vogensen S, Howe J. The relationship between agonist potency and AMPA receptor kinetics. Biophys J. 2006; 91:1336–1346. [PubMed: 16731549]
38. Schorge S, Elenes S, Colquhoun D. Maximum likelihood fitting of single channel NMDA activity with a mechanism composed of independent dimers of subunits. J Physiol. 2005; 569:395–418. [PubMed: 16223763]
39. Amico-Ruvio SA, Popescu GK. Stationary Gating of GluN1/GluN2B Receptors in Intact Membrane Patches. Biophys. J. 2010; 98:1160–1169. [PubMed: 20371315]
40. Blanke ML, VanDongen AMJ. Constitutive activation of the N-methyl-D-aspartate receptor via cleft-spanning disulfide bonds. J. Biol. Chem. 2008; 283:21519–21529. [PubMed: 18450751]

41. Colquhoun D, Sakmann B. Fast events in single-channel currents activated by acetylcholine and its analogues at the frog muscle end-plate. J Physiol. 1985; 369:501–557. [PubMed: 2419552]
42. Edmonds B, Gibb AJ, Colquhoun D. Mechanisms of activation of glutamate receptors and the time course of excitatory synaptic currents. Annu Rev Physiol. 1995; 57:495–519. [PubMed: 7778875]
43. Colquhoun D. Agonist-activated ion channels. Br J Pharmacol. 2006; 147(Suppl 1):S17–26. [PubMed: 16402101]
44. Colquhoun D. Binding, gating, affinity and efficacy: the interpretation of structure-activity relationships for agonists and of the effects of mutating receptors. Br J Pharmacol. 1998; 125:924–947. [PubMed: 9846630]
45. Colquhoun D, Large WA, Rang HP. An analysis of the action of a false transmitter at the neuromuscular junction. The Journal of Physiology. 1977; 266:361–395. [PubMed: 192885]
46. Pan Z, Tong G, Jahr CE. A false transmitter at excitatory synapses. Neuron. 1993; 11:85–91. [PubMed: 8101712]
47. Erreger K, et al. Mechanism of Partial Agonism at NMDA Receptors for a Conformationally Restricted Glutamate Analog. J. Neurosci. 2005; 25:7858–7866. [PubMed: 16120788]
48. Kussius CL, Popescu GK. Kinetic basis of partial agonism at NMDA receptors. Nat Neurosci. 2009; 12:1114–1120. [PubMed: 19648915]
49. Chen PE, et al. Modulation of glycine potency in rat recombinant NMDA receptors containing chimeric NR2A/2D subunits expressed in Xenopus laevis oocytes. J Physiol. 2008; 586:227–245. [PubMed: 17962328]
50. Furukawa H, Singh SK, Mancusso R, Gouaux E. Subunit arrangement and function in NMDA receptors. Nature. 2005; 438:185–192. [PubMed: 16281028]
51. Armstrong N, Gouaux E. Mechanisms for activation and antagonism of an AMPA-sensitive glutamate receptor: crystal structures of the GluR2 ligand binding core. Neuron. 2000; 28:165–181. [PubMed: 11086992]
52. Mayer ML, Ghosal A, Dolman NP, Jane DE. Crystal Structures of the Kainate Receptor GluR5 Ligand Binding Core Dimer with Novel GluR5-Selective Antagonists. J. Neurosci. 2006; 26:2852–2861. [PubMed: 16540562]
53. Traynelis SF, Burgess MF, Zheng F, Lyuboslavsky P, Powers JL. Control of voltage-independent zinc inhibition of NMDA receptors by the NR1 subunit. Journal of Neuroscience. 1998; 18:6163–6175. [PubMed: 9698310]
54. Erreger K, Traynelis SF. Allosteric interaction between zinc and glutamate binding domains on NR2A causes desensitization of NMDA receptors. J Physiol. 2005; 569:381–393. [PubMed: 16166158]
55. Christopoulos A. Assessing the distribution of parameters in models of ligand-receptor interaction: to log or not to log. Trends Pharmacol Sci. 1998; 19:351–357. [PubMed: 9786022]
56. McCoy AJ, et al. Phaser crystallographic software. J. Appl. Cryst. 2007; 40:658–674. [PubMed: 19461840]
57. Adams PD, et al. PHENIX: building new software for automated crystallographic structure determination. Acta Crystallogr D Biol Crystallogr. 2002; 58:1948–1954. [PubMed: 12393927]
58. Emsley P, Cowtan K. Coot: model-building tools for molecular graphics. Acta Crystallogr D Biol Crystallogr. 2004; 60:2126–2132. [PubMed: 15572765]

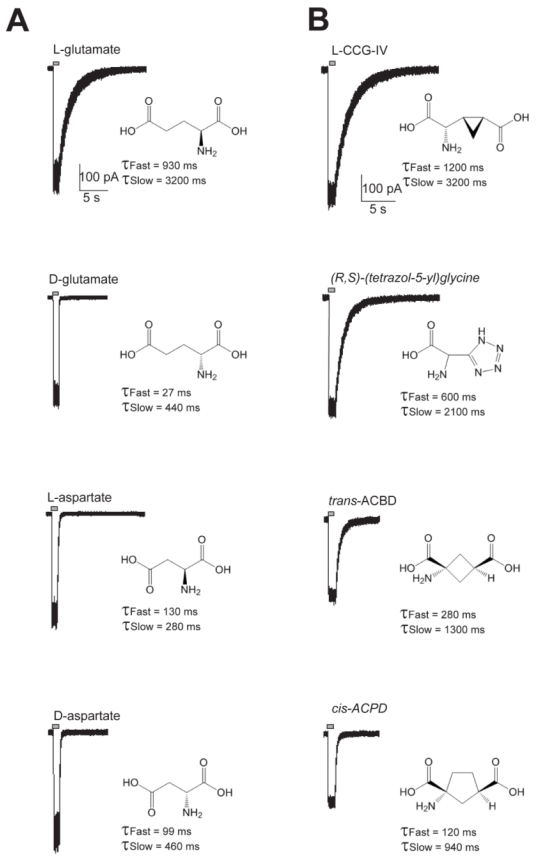

Figure 1.

Deactivation time course of GluN1/GluN2D NMDA receptors is dependent on the structure of the activating ligands. HEK 293 cells were activated under voltage-clamp by maximally effective concentrations of various linear agonists (panel *A*; L-glutamate, D-glutamate, L-aspartate, and D-aspartate) and cyclic agonists (panel *B*; L-CCG-IV, *trans*-ACBD, (*RS*)-(tetrazol-5-yl)glycine, and *cis*-ACPD) applied for 1 s; all solutions contained 0.05 mM glycine. L-glutamate and L-CCG-IV evoked the slowest deactivation time courses of the ligands examined. All other linear and cyclic agonists evoked significantly more rapid deactivation time courses than L-glutamate or L-CCG-IV. The deactivation time constants are given as the mean of 5-26 cells.

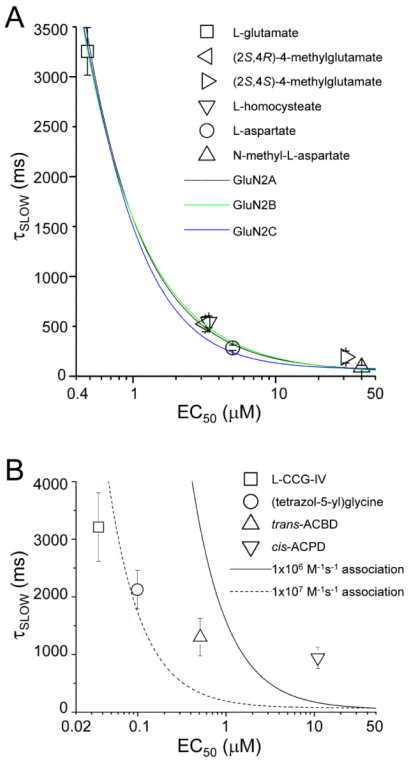

Figure 2.

The relationship between deactivation and EC_{50}. ***A***, The relationship between the experimentally-determined τ_{SLOW} and the EC_{50} value for the steady-state response is shown for linear ligands for which τ_{SLOW} contributes greater than 10% to the time course (L-glutamate, L-homocysteate, L-aspartate, NMLA, (2*S*,4*R*)-4-methylglutamate, and (2*S*,4*S*)-4-methylglutamate). Super-imposed on these data are simulated response properties from an NMDA receptor gating model for GluN1/GluN2A previously described by Schorge et al. (2005)[38] as well as published models for GluN1/GluN2B[39] and GluN1/GluN2C[26], adapted for L-glutamate-activated GluN1/GluN2D receptors by removal of the desensitized states (see *Methods*). We first determined association and dissociation rate constants that yielded a steady-state EC_{50} and deactivation time constant similar to that measured for L-glutamate-activated GluN1/GluN2D. We subsequently simulated the responses of each adapted model using an association rate (b_+) of 1.0×10^6 $M^{-1}s^{-1}$. The dissociation rates (b_-) were varied between 0.1 to 100 s^{-1} while holding the gating rates constant. The solid lines show the relationship between the EC_{50} value and tau deactivation for each adapted model. ***B***, The relationship between experimentally determined EC_{50} values and τ_{SLOW} for the cyclic ligands is shown. Superimposed on this plot is the relationship between tau deactivation and the EC_{50} value predicted for L-glutamate activation of the GluN1/GluN2A adapted model as dissociation rates vary between 0.5 to 100 s^{-1} (solid line). Simulations using the same rate constants and a faster association rate (1.0×10^7 $M^{-1}s^{-1}$) are shown (broken line; gating rates held constant). The faster association rates provided a better prediction of the τ_{SLOW} of L-CCG-IV and (*RS*)-(tetrazol-5-yl)glycine, but did not predict the deactivation time courses of *trans*-ACBD, and *cis*-ACPC.

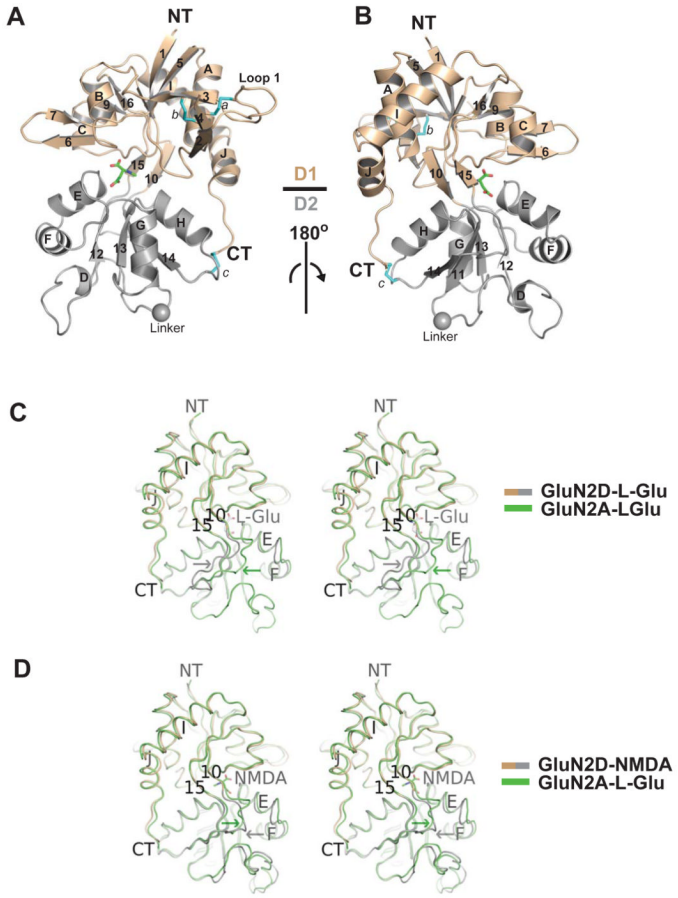

Figure 3.

Crystal structure of GluN2D ligand-binding domain. *A and B*, Overall structure of the bilobed GluN2D ligand-binding domain in complex with NMDA (green sticks) is shown with the N-terminus (NT) and C-terminus (CT) on top and bottom, respectively. Ligands such as NMDA bind to the inter-domain cleft between domain 1 (D1; wheat) and domain 2 (D2; light gray). Three disulfide bonds (*a*-*c*; cyan sticks) are formed between the following cysteine pairs: Cys452 and Cys490 (*a*), Cys459 and Cys481 (*b*), and Cys770 and Cys825 (*c*). The sphere indicated as 'linker' is the Cα of glycine in the Gly and Thr residues that replace the transmembrane domains. *C*, Structural comparison between L-glutamate bound to GluN2D (wheat and light gray) and GluN2A (PDB code: 2A5S, green) in stereo view. The superposition shows divergent region, Hinge loop (green arrow: GluN2A; and gray arrow: GluN2D), proximal to helices E and F and strands 15 and 16. The orientation of the structures is the same as in panel *B*. *D*, Structural comparison between NMDA-bound GluN2D (wheat and light gray) and L-glutamate-bound GluN2A (green) in stereo view. The superposition shows a similarity in orientation of hinge loops (arrows) between GluN2A and GluN2D. The root-mean-square deviation of superposition is1.10 Å over 263 Cα positions. Disulfide bonds are omitted for clarity in panel *C* and *D*.

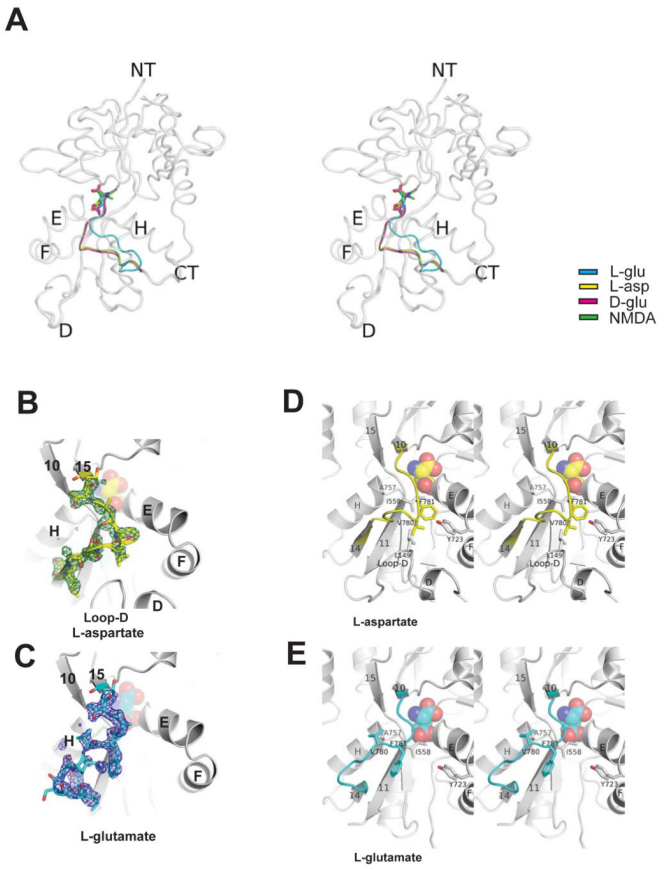

Figure 4.

Conformational variability at the clamshell hinge. *A*, Stereo view of the overall structures of GluN2D ligand-binding domain in complex with various ligands. The structural superposition reveals a distinct conformation of hinge loops (colored loops) between the L-glutamate bound form (cyan) and all the other forms (L-aspartate = yellow, D-glutamate = magenta, and NMDA = green). Ligands are shown as sticks. *B and C*, *Fo-Fc* omit electron density of "hinge loop" contoured at 2.8σ for the L-aspartate-(panel *B*) and L-glutamate-bound (panel *C*) structures. The residues are well ordered except for a portion of Lys779, as shown by a breakage at the electron density map. *D and E*, Different modes of interactions between "hinge loop" and Helices E-F or Helix H in the L-aspartate-bound (*panel* D) and L-glutamate-bound (*panel* E) structures. The loop that contains Leu690 in the L-aspartate-bound structure (Loop-D) and Helix D are disordered in the L-glutamate-bound structure. Ligands are shown as spheres. Residues on the hinge loops are colored as yellow and cyan for L-aspartate-bound and L-glutamate-bound structures, respectively. Residues proximal to the hinge loop are in white.

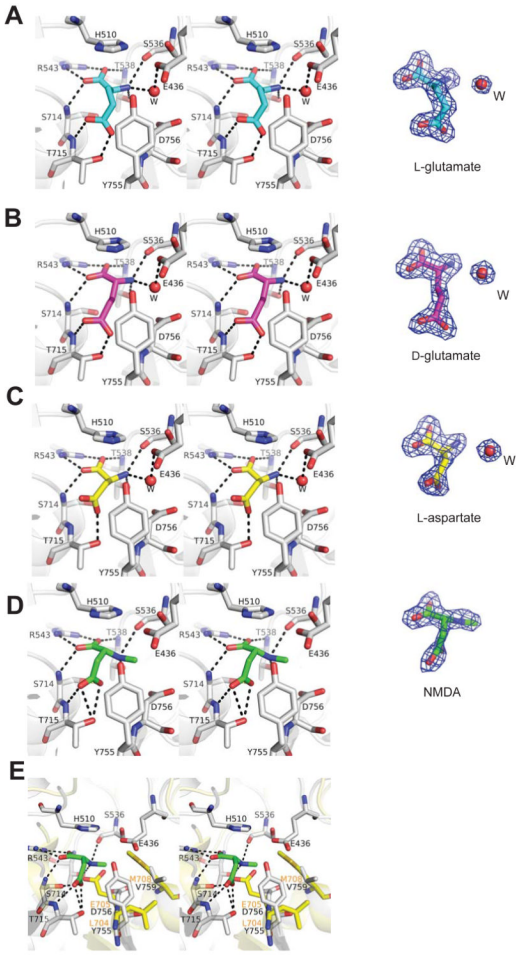

Figure 5.

Agonist binding site of GluN2D and molecular determinants for NMDA specificity. *A-D*, All of the ligands tested in this study bind inter-domain cleft between domains D1 and D2. Shown here are stereo views of the ligand-binding site of GluN2D in complex with L-glutamate (*A*; in cyan), D-glutamate (*B*: in magenta), L-aspartate (*C*; in yellow), and NMDA (*D*; in green). A water molecule (W) present in the L-glutamate, D-glutamate, and L-aspartate binding pocket is represented by a red sphere. Shown on the right hand side of panel *A-D* in blue mesh are *Fo-Fc* omit difference Fourier maps for the ligands and the attached water molecule contoured at 4σ. *E*, Structures of GluN2D ligand-binding domain (gray) and GluA2 ligand-binding domain (PDB code: 1FTJ; in yellow) are superimposed to one another to show unfavorable placement of NMDA molecule (green) in non-NMDA receptors. Corresponding residues of GluN2D Tyr755, Asp756 and Val759 in GluA2 are Leu704, Glu705 and Met708 (in yellow), respectively. A placement of *N*-methyl group of NMDA is favored in the GluN2 subunit due to the hydrophobic environment created by Tyr755 and Val759 and due to the location of the Asp756 side chain away from the pocket. In AMPA receptor, the equivalent residue to Asp756 is glutamate (Glu705) whose longer side chain would collide with the *N*-methyl group. The binding is also disfavored due to replacement of Val759 with methionine, which makes the binding pocket less hydrophobic.

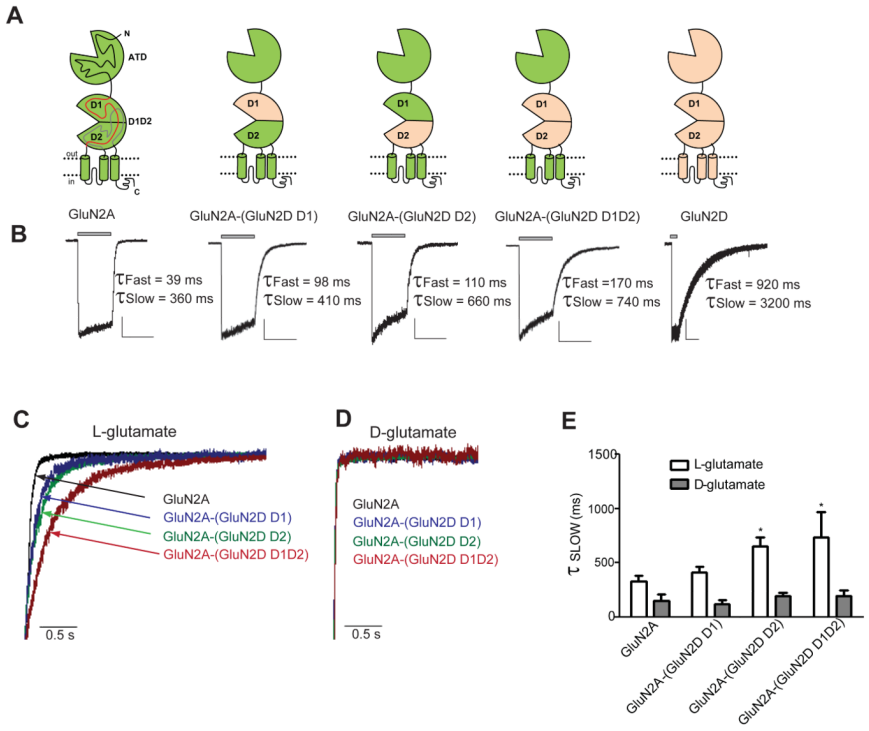

Figure 6.

Assessment of molecular determinants within ligand-binding domain for controlling GluN2D deactivation time course using GluN2A-GluN2D receptors. *A*, Cartoons of the wild type and chimeric receptors are given, with GluN2A in green and GluN2D in wheat. *B*, L-glutamate (1 mM) was applied rapidly to transfected HEK 293 cells for 1 s (gray bars); 0.05 mM glycine was present in all solutions. Inserting portions or the GluN2D D1D2 ligand-binding domain increased the fast and slow time constants describing the deactivation time course compared to the time constants of GluN1/GluN2A. The horizontal scale bar represents 2 sec for all traces, and the vertical scale bar represents approximately 200 pA for all traces. *C*, Normalized current traces of the deactivation time courses of GluN2A and chimeric receptors following removal of L-glutamate. *D*, Normalized current traces of GluN2A and chimeric receptors following the removal of D-glutamate. The deactivation time course following removal of D-glutamate did not significantly lengthen for any chimeric receptor. *E*, The slow deactivation time constant (τ_{SLOW}) of GluN2A and the chimeric receptors is given for L-glutamate (white bars) and D-glutamate (gray bars). Bars are given in mean ± s.e.m. *p<0.05 when compared to the deactivation time course of GluN1/GluN2A activated by L-glutamate and analyzed by one-way ANOVA with Tukey's *post hoc* test.

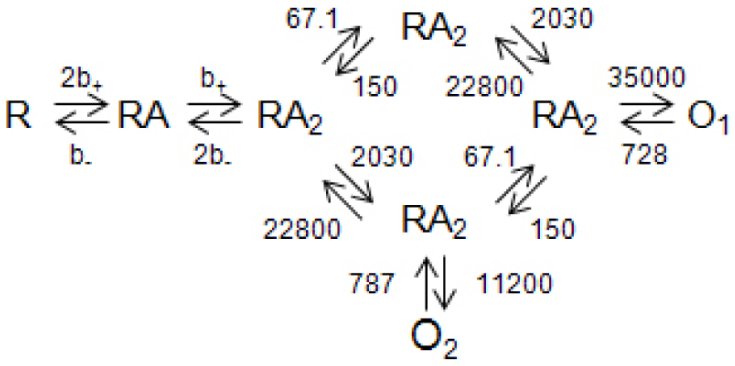

Scheme 1.

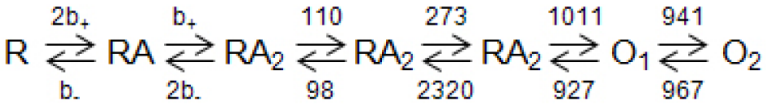

Scheme 2.

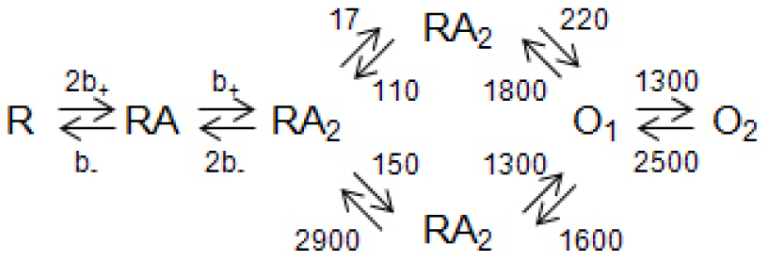

Scheme 3.

Table 1

Summary of deactivation time course of GluN1/GluN2D receptors activated by linear glutamate and aspartate analogues

Ligand	τ_{FAST} (ms)	τ_{SLOW} (ms)	τ_W(ms)	% fast	n	EC_{50} (μM)
L-glutamate	930 ± 100	3200 ± 240	2300 ± 96	37 ± 4.3	30	0.48
D-glutamate	27 ± 2.4*	440 ± 120*	42 ± 4.8*	93 ± 2.4*	12	42
L-aspartate	130 ± 10*	280 ± 25*	160 ± 4.5*	74 ± 7.9*	8	5.0
D-aspartate	99 ± 8.3*	460 ± 100*	130 ± 13*	90 ± 1.5*	7	2.1
N-methyl-L-aspartate	17 ± 4.5*	91 ± 18*	38 ± 2.5*	62 ± 11	6	40
N-methyl-D-aspartate	60 ± 2.2*	280 ± 36*	75 ± 3.4*	93 ± 1.9*	5	7.3
L-homocysteate	160 ± 27*	540 ± 59*	370 ± 23*	43 ± 9.7	5	3.4
D-homocysteate	35 ± 2.9*	300 ± 97*	45 ± 3.2*	91 ± 4.0*	10	22
(2S,4R)-4-methylglutamate (SYM 2081)	130 ± 32*	520 ± 76*	330 ± 47*	48 ± 9.5	5	3.2
(2S,4S)-4-methylglutamate	25 ± 5.0*	190 ± 59*	56 ± 10*	66 ± 15	5	31

τFAST, τSLOW, τW, and % fast values are shown as mean ± s.e.m.; n is the number of cells. Values are given to two significant figures. All EC50 values except L-glutamate and L-aspartate are from Erreger et al. (2007)[36].

*$p<0.05$ compared to L-glutamate; one-way ANOVA with Tukey's *post hoc* test.

Table 2

Summary of the deactivation time course of GluN1/GluN2D receptors activated by cyclic glutamate analogues

Ligand	τ_{FAST} (ms)	τ_{SLOW} (ms)	τ_W(ms)	% fast	n	EC_{50} (μM)
L-glutamate	930 ± 100	3200 ± 240	2300 ± 96	37 ± 4.3	30	0.48
L-CCG-IV	1200 ± 290	3200 ± 600	2500 ± 370	32 ± 4.5	5	0.036
(RS)-(tetrazol-5-yl)glycine	600 ± 140	2100 ± 340	1400 ± 190*,#	42 ± 12	5	0.099
***trans*-ACBD**	280 ± 69*,#	1300 ± 320*	620 ± 77*,#	59 ± 10	5	0.51
***cis*-ACPD**	120 ± 23*,#	940 ± 190*,#	350 ± 88*,#	72 ± 11	5	11

τFAST, τSLOW, τW, and % fast values are shown as mean ± s.e.m., and n is the number of cells. Values are given to two significant figures. All EC_{50} values except L-glutamate are from Erreger et al. (2007)[36].

*$p < 0.05$ when compared to L-glutamate (one-way ANOVA with Tukey's *post hoc* test).

#$p < 0.05$ when compared L-CCG-IV (one-way ANOVA with Tukey's *post hoc* test).

Table 3

Summary of the deactivation time course of GluN1/GluN2A receptors activated by glutamate and aspartate analogues

Ligand	τ_{FAST} (ms)	τ_{SLOW} (ms)	τ_W(ms)	% fast	n	EC_{50} (μM)
L-glutamate	38 ± 1.7	330 ± 50	54 ± 3.2	88 ± 4.0	21	4.5
D-glutamate	16 ± 1.3*	280 ± 130	22 ± 3.0*	95 ± 1.9	7	250
L-aspartate	20 ± 2.5*	340 ± 72	32 ± 6.1*	96 ± 1.4	7	48
D-aspartate	26 ± 3.3	810 ± 540	35 ± 6.5	83 ± 9.2	6	30
N-methyl-L-aspartate	9.5 ± 1.4*	170 ± 130	11 ± 1.3*	96 ± 3.0	6	580
N-methyl-D-aspartate	16 ± 1.8*	320 ± 58	20 ± 2.1*	98 ± 1.4	4	94
L-homocysteate	15 ± 3.5*	430 ± 190	31 ± 6.9	80 ± 17	5	34
D-homocysteate	15 ± 3.0*	290 ± 16	22 ± 3.1*	98 ± 0.22	4	180
(2S,4R)-4-methylglutamate (SYM 2081)	39 ± 4.2	350 ± 49	52 ± 5.6	95 ± 18	5	144
(2S,4S)-4-methylglutamate	11 ± 1.0*	47 ± 15	13 ± 1.2*	93 ± 3.9	5	404
L-CCG-IV	54 ± 7.2*	240 ± 43	70 ± 8.4	89 ± 5.8	5	0.26
(*R,S*)-(tetrazol-5-yl)glycine	60+ 8.2*	300 ± 58	89 ± 9.0*	84 ± 6.8	5	1.7
***Trans*-ACBD**	40 ± 5.4	420 ± 77	59 ± 6.0	96 ± 0.98	5	3.1
***Cis*-ACPD**	39 ± 4.2	350 ± 49	52 ± 5.6	95 ± 1.9	5	61

τFAST, τSLOW, τ_W, and % fast values are shown as mean ± s.e.m., and n is the number of cells. Values are given to two significant figures. All EC_{50} values except L-glutamate are from Erreger et al. (2007)[36].

*p<0.05 when compared to GluN1/GluN2A activated by L-glutamate and analyzed by one-way ANOVA with Tukey's *post hoc* test.

Table 4

GluN2A-GluN2D chimeric receptors activated by L-glutamate

Receptor	τ_{FAST} (ms)	τ_{SLOW} (ms)	τ_W(ms)	% fast	n	EC_{50}
GluN2A WT	39 ± 1.8	360 ± 53	54 ± 3.5	89 ± 4.4	21	4.5 ± 0.42
GluN2A-(GluN2D D1)	98 ± 4.7*	410 ± 56	150 ± 11	80 ± 7.1	5	0.68 ± 0.20**
GluN2A-(GluN2D D2)	110 ± 5.6*	660 ± 83*	160 ± 4.5*	88 ± 2.7	7	1.2 ± 0.2**
GluN2A-(GluN2D D1D2)	170 ± 35*	740 ± 230*	280 ± 42*	72 ± 8.0	5	0.44 ± 0.082**
GluN2D WT	930 ± 100*	3200 ± 240*	2300 ± 96*	37 ± 4.3*	30	0.48

τFAST, τSLOW, τ_W, % fast, and EC_{50} values are shown as mean ± s.e.m. n is the number of cells for deactivation measurements; EC_{50} values were determined in 4-6 oocytes for each receptor. All data are given to two significant figures.

* $p<0.05$ when compared to GluN1/GluN2A activated by L-glutamate and analyzed by one-way ANOVA with Tukey's *post hoc* test.

** $p<0.05$ when log(EC50) is compared to the log(EC50) for L-glutamate activation of GluN1/GluN2A, analyzed by one-way ANOVA with Tukey's *post hoc* test (see Methods).

Table 5

GluN2A and GluN2D point mutant receptors activated by L-glutamate

Receptor	τ_{FAST} (ms)	τ_{SLOW} (ms)	τ_W(ms)	% fast	n
GluN2A WT	38 ± 1.7	330 ± 50	54 ± 3.2	88 ± 4.0	21
GluN2A-Y754K	110 ± 7.5*	950 ± 150*	170 ± 18*	91 ± 1.3	20
GluN2A-Y754K, I755V	32 ± 1.5	370 ± 60	55 ± 4.6	90 ± 2.6	12
GluN2D WT	930 ± 100	3200 ± 240	2300 ± 96	37 ± 4.3	30
GluN2D-K779Y	670 ± 150	2900 ± 260	2200 ± 94	32 ± 6.5	9
GluN2D-V780I	440 ± 170	4800 ± 630	4100 ± 630^	17 ± 4.1	5
GluN2D-K779Y, V780I	1100 ± 170	4400 ± 400	3300 ± 190^	34 ± 6.6	5

τFAST, τSLOW, τ_W, and % fast values are shown as mean ± s.e.m., and n is the number of cells. All data are given to two significant figures.

*p<0.05 when compared to GluN1/GluN2A activated by L-glutamate and analyzed by oneway ANOVA with Tukey's *post hoc* test.

^p<0.05 when compared to the deactivation time course of GluN1/GluN2D activated by L-glutamate and analyzed by one-way ANOVA with Tukey's *post hoc* test.